

Hubble Space Telescope Observations of Star Clusters in M101¹

Pauline Barmby

*Harvard-Smithsonian Center for Astrophysics, 60 Garden St., Mailstop 65, Cambridge,
MA 02138*

pbarby@cfa.harvard.edu

K.D. Kuntz

*The Henry A. Rowland Department of Physics and Astronomy, The Johns Hopkins
University, 400 Charles Street, Baltimore MD 21218 and Exploration of the Universe
Division, X-Ray Astrophysics Laboratory, Code 662, NASA Goddard Space Flight Center,
Greenbelt, MD 20771*

John P. Huchra

Harvard-Smithsonian Center for Astrophysics, 60 Garden St., Cambridge, MA 02138

Jean P. Brodie

UCO/Lick Observatory, University of California, Santa Cruz, CA 95064

ABSTRACT

Hubble Space Telescope Advanced Camera for Surveys (ACS) images are used to identify and study star cluster candidates in the nearby spiral galaxy M101. About 3000 round, slightly-resolved cluster candidates are identified in 10 ACS pointings covering an area of 106 arcmin². The cluster candidates' color and size distributions are consistent with those of star clusters in other nearby spirals. The majority of the M101 candidates are blue and more likely to be associated with the galaxy's spiral arms, implying that they are young. The galaxy-luminosity-normalized number of 'young massive clusters' in M101 is similar to that found in other spirals, as is the cluster density at a fiducial absolute magnitude. We confirm a previous finding that M101 has a large number of faint, red star clusters: if these are old globular clusters then this galaxy has a very large globular cluster population. More plausible is that the faint red clusters are reddened young clusters; their colors and luminosities are also consistent with this explanation.

Subject headings: galaxies: individual (M101) — galaxies: star clusters — galaxies:spiral

1. Introduction

Understanding the stellar populations of galaxies is key to untangling the mysteries of their formation and evolution. Because of our location in the Milky Way, getting an overall picture of the stellar populations is difficult. The nearby spiral galaxy M101 (NGC 5457) is the closest face-on spiral (Hubble type SAB(rs)cd; de Vaucouleurs et al. 1991) and provides an excellent opportunity for resolution of stellar population details. Previous studies of stellar populations in M101 include work on the Cepheid variable stars (Kelson et al. 1996; Stetson et al. 1998), X-ray binaries (Kuntz et al. 2005; Mukai et al. 2003), and novae (Shafter et al. 2000), among many others.

Star clusters are excellent tracers of stellar populations: they are much brighter than single stars and usually have small internal spreads in age and metallicity. Globular clusters in particular are believed to be indicators of galaxy history (e.g., Strader et al. 2005). Globular cluster systems (GCSs) in spirals have been studied much less than their counterparts in ellipticals: spirals have fewer clusters per unit of galaxy light, and their irregular background light makes detection of clusters more challenging. The Milky Way GCS is the ‘gold standard’ for comparison to all others, but it is difficult to say whether it is a truly typical GCS since the sample of spiral galaxy GCSs available for comparison is small. Younger star cluster populations are better-studied in other galaxies (e.g., Larsen & Richtler 1999) than in the Milky Way; due to extinction, the census of young cluster populations in the Galaxy is far from complete (Bica et al. 2003).

Studying clusters in edge-on spirals (e.g., Goudfrooij et al. 2003) ameliorates the background light issue, but the nearest such galaxies are distant enough that their star clusters are unresolved; confirmation that candidates are true clusters is difficult. Recently, *Hubble Space Telescope* (HST) imaging has been used to search for star clusters in a number of low-inclination nearby spiral galaxies, including M81 (Chandar et al. 2001a, Nantais et al., 2006 in preparation), M51 (Bik et al. 2003; Lee et al. 2005), and these two galaxies plus M83, NGC 6946 and M101 (Chandar et al. 2004). The high spatial resolution of HST images aids in distinguishing true clusters from contaminants such as background galaxies and multiple star blends and improves photometric precision. The HST studies mentioned above have generally covered only small regions of these nearby galaxies using one or two HST pointings. Here we complement these works by presenting initial results from a study

¹Based on observations made with the NASA/ESA Hubble Space Telescope, obtained at the Space Telescope Science Institute, which is operated by the Association of Universities for Research in Astronomy, Inc., under NASA contract NAS 5-26555. These observations are associated with programs #8640 and #9490.

of star clusters found in ten HST/ACS fields in M101, covering a much larger fraction of the galaxy. Throughout this work we assume a distance to M101 of 6.7 Mpc ($m - M = 29.13$; Freedman et al. 2001). At this distance, one arcsecond subtends 32.5 pc.

2. Observations and cluster selection

Images of 10 fields in M101 (see Figure 1) were taken with the Wide Field Camera of the Advanced Camera for Surveys (Ford et al. 2002) on HST, during the period 2002 November 13–16. Each field was observed for 900 s in the F435W filter and 720 s each in F555W and F814W; the exposures were ‘cosmic-ray-split’ but not dithered. The pipeline-processed, drizzled versions of the data retrieved in 2003 February were used in this analysis. The $S/N = 10$ detection limit for point sources in these data is given by the ACS exposure time calculator as $B = 25.7$, $V = 25.4$, $I = 25.0$. The total area covered by our survey is about 106 arcmin²; this accounts for the overlap between the ACS pointings and the missing area in the ACS inter-chip gaps.

Even a casual inspection of the images reveals a wealth of detail (e.g., see Figure 2), and an initial attempt at source extraction yielded tens of thousands of detected objects per field. The expected population of M101 star clusters includes a few hundred globular clusters and a few thousand younger clusters, so finding these requires care and attention. Although automatic selection can reduce the number of cluster candidates to a manageable one, we found that human judgment was required in the final selection.

Star clusters in M101 were expected to be slightly resolved in HST images: a typical Milky Way globular cluster half-light radius of 3.2 pc corresponds to about 2 ACS/WFC pixels. Unfortunately there are many other sources which are slightly resolved in the images, including background galaxies, H II regions, blended stars, etc. To understand what star clusters in M101 might look like, we modeled their appearance using HST images of M31 globular clusters. The M31 cluster images were taken with STIS as part of program GO-8640, designed to measure structural parameters for the clusters. We chose six clusters with a range of sizes and shapes, and modeled their appearance in ACS images of M101 using version 6.0 of TinyTIM (Krist 1995). M31 is about 10 times closer than M101, so the STIS images were input to TinyTIM as 10-times oversampled images, then convolved with the HST/ACS point spread function using TinyTIM’s “scene-generation” facility. Appropriate PSFs for the three ACS filters were used, but no attempt was made to model the color-dependence of cluster appearance; the wide bandpass of the STIS 50CCD filter made this unnecessary. We computed PSFs and modeled artificial M101 clusters on a grid of 144 positions on the ACS WFC detectors.

The artificial clusters were used first to define the cluster-selection procedure. We chose V magnitudes randomly from a Gaussian with mean 22.0 and dispersion 1.2, $B - V$ and $V - I$ colors from Gaussians with means of 0.72 and 0.96 and dispersion 1.2, and reddening from a uniform distribution with $0 < E(B - V) < 0.2$. The clusters were then added into the ACS images of field 1 (the innermost pointing) on their PSF grid positions. After experimenting with object detection and measurement schemes, we decided to use SExtractor (Bertin & Arnouts 1996) for object detection and measurement,² followed by FWHM measurements with the IRAF task APPHOT.RADPROF. Final cluster candidate selection criteria were: objects which appear in all three of B , V , and I , with $\text{MAG_BEST} < 23.5$, $\text{CLASS_STAR} < 0.05$, and $\text{ELLIP} < 0.5$ as measured on the I images, and $2.2 < \text{FWHM} < 6$ pixels as measured by RADPROF. Adding the magnitude criterion ensured that objects would be bright enough for shape measurements and star/galaxy classifications to be meaningful. Adding the FWHM criterion removed many extended sources which appeared to be galaxies, reducing the number of candidates to a manageable level while retaining most of the inserted artificial clusters. The upper limit on FWHM of 6 pixels corresponds to an effective radius $R_e = 14.4$ pc (see Section 3.3) at the distance of M101.

The actual cluster-finding procedure consisted of applying the above criteria to each of the ten fields. Before finding clusters, we inserted 20 artificial clusters in each field. The same scheme described above was used, except that the cluster locations were chosen randomly and the cluster image used was the one with the closest PSF location. After doing object detection and applying the cluster criteria, the remaining candidates were visually examined to remove objects which appeared to be background galaxies or blended stars. The visual inspection imparts some subjectivity to the selection procedure; however it proved to be necessary since we were unable to define an automatic selection procedure which was both complete (picking out most of the artificial clusters) and reliable (not picking too many obvious contaminants). The fraction of candidates removed by the visual selection ranged from almost 50% in the central field to about 30% in the outer fields.

The completeness of the selection procedure is not well-defined because of the subjective visual inspection. However, it can be estimated by considering the fraction of artificial clusters which survived the selection procedure. This ranged from 70% in the central field to 90% in several of the outer fields, with an average of 83%. A few clusters were missed because they were inserted at magnitudes beyond the cutoff; most of the rest were deleted by the visual inspection procedure, usually because they were not quite compact enough to

²SExtractor parameters were set to the following values: $\text{SEEING_FWHM } 0''.1$, $\text{DETECT_MINAREA}=4$, $\text{DETECT_THRESH}=1.5$, and the images were convolved with a 5×5 pixel Gaussian filter before object detection.

look like distinct objects. The final result of the cluster selection procedure was a list of 2920 candidates. Images of a few candidates chosen at random from the final list are shown in Figure 3. The cluster candidates are reasonably round and appear resolved compared to nearby stars; further analysis of their light distribution is in Section 3.3.

Photometry of the cluster candidates was extracted from the SExtractor output. Total magnitudes were measured with the SExtractor MAG_AUTO estimator. Colors were measured using aperture magnitudes in 2.5 pixel radius apertures. The aperture magnitudes were corrected to large apertures using aperture corrections derived from the clusters themselves; since the clusters are slightly resolved, corrections based on the instrument point spread function alone are inappropriate. Corrections used were -0.905 , -0.941 , and -1.055 magnitudes in the F435W, F555W, and F814W filters, respectively. Transformations to the standard Johnson-Cousins system were made using the equations and parameters in Sirianni et al. (2005); no corrections for charge transfer efficiency were made, but these are expected to be small since the observations were made early in the life of ACS.

We used the H I column density map given by Kuntz et al. (2003) and a dust-to-gas ratio of $E(B - V) = 1.72 \times 10^{-22} N(\text{HI} + \text{H}_2)$ (Bohlin et al. 1978) to de-redden the colors of the M101 cluster candidates. The column density map reflects the total absorbing column in the M101 disk, so this correction will over-estimate the reddening for objects in front of the disk plane (i.e., some globular clusters.) Without further information, there is no way to tell which clusters are in front of the disk and which are behind, and the reddening corrections are mostly small (the median value in the area covered by the ACS images is $E(B - V) = 0.05$, with a maximum value of 0.26). Galactic extinction in the direction of M101 is very low ($E(B - V) < 0.01$; Chandar et al. 2004) so we do not correct for it.

We can compare the results of our selection with the study of Bresolin et al. (1996, hereafter BKS). These authors performed a visual search for clusters in one HST/WFPC2 field which is contained within our central ACS pointing.³ Their 43 cluster candidates have a median V magnitude of 21.5. Two of their candidates fall in the gap between the ACS detectors, and two are not identifiable on the WFPC2 image. In the same area searched by BKS, our cluster selection procedure picked 232 candidates with a median magnitude of $V = 22.8$. Twenty-two of the remaining 39 BKS candidates (56%) are in our candidate list. Visual examination of the 17 BKS clusters not in our list shows them to have a range of morphologies, but they are generally less round and less isolated than the clusters on

³We discovered that the coordinates given for BKS' clusters 30–43 do not fall on any obvious objects in the ACS image; it appears that these objects fall on the WF4 chip, but their RA and Dec were computed using the world coordinate system for the PC1 image. With the correct transformations all except two of the coordinate pairs fall on obvious cluster candidates in the WF4 image.

our list (see also Figure 2). As indicated by the median magnitudes, our candidates are generally fainter than those of BKS. Comparison of photometry for objects in common shows a small offset: median differences between their photometry and ours are $\Delta V = 0.16 \pm 0.04$, $\Delta(B - V) = -0.14 \pm 0.03$, and $\Delta(V - I) = +0.08 \pm 0.03$. BKS state that their magnitudes are uncertain by ≥ 0.1 mag, so we do not believe the offset indicates a serious problem in our photometry.

3. Analysis

Star cluster system studies have generally focused on two separate populations: the old, globular clusters or the young, massive clusters. Elliptical galaxies, of course, have only the first type of cluster, while the clusters studied in galaxy mergers exemplify the second. The color distribution of the M101 cluster candidates is expected to reflect their age distribution: while colors of globular clusters are often used as indicators of metallicity (e.g. Kundu & Whitmore 1998), many of the M101 candidates are far too blue to be old, metal-poor clusters. In the following analysis, we will use color as a simple observational distinction between older and younger clusters, to ease comparison with other star cluster studies. $B - V = 0.45$ is the red limit used by Larsen & Richtler (1999) for their studies of ‘Young Massive Clusters’, and is also close to the blue limit of the Milky Way globular cluster $(B - V)_0$ distribution, so we adopt $(B - V)_0 = 0.45$ as the dividing line between old and young clusters. It should be remembered, however, that the age distribution of star clusters in M101 is not necessarily bimodal, and this division is somewhat arbitrary. More precise age estimates will be enabled with the use of UV and/or $H\alpha$ imaging; such data already exist for a portion of the observed field and will be utilized in a future paper.

Of the 2920 star cluster candidates in our sample, 1877 (65%) are blue, with $(B - V)_0 < 0.45$. The effect of our $I = 23.5$ magnitude limit is such that our cluster sample contains faint clusters only if they are red. The bluest clusters in our sample have $V - I \approx -0.5$, so the sample is not color-biased above $V = 23$ ($M_V = -6.1$). To this limit, there are 1715 cluster candidates of which 1260 (73%) are blue. Figure 4 shows the spatial distribution of the M101 candidates, both the complete sample and the bright ($V < 23$) red and blue subsamples. The spiral pattern of the galaxy is more apparent in the blue clusters. This is consistent with them being younger and associated with star formation in the spiral arms, and indeed the bluest clusters ($(B - V) < 0.2$) trace the arms even more clearly.

3.1. Color and luminosity distributions

Observed color distributions for the candidates are shown in Figure 5. The left panel of this figure compares the colors for M101 clusters to those in other nearby spirals: M81 (Chandar et al. 2001a), M33 (Mochejska et al. 1998), and M51 (Bik et al. 2003); these colors have not been corrected for reddening. The color distribution of M101 candidates is most similar to that of the M33 candidates, which is unsurprising given that the two galaxies are the same Hubble type and have a similar specific star formation rate. M101 has fewer blue clusters than M51 and fewer red clusters than M81. This is broadly consistent with a picture in which the proportion of blue to red clusters reflects the recent star formation rate (M51 might be expected to have enhanced star formation due to encounters with its companion), and the number of red clusters is proportional to the galaxy bulge mass (which is larger for M81, an earlier-type galaxy than M101). Chandar et al. (2001b) interpret the separation of M81 cluster colors into two groups (at $B - V \approx 0.5$ and $V - I \approx 1.0$) as a separation in age. No such clear separation is apparent in the M101 cluster candidates.

In the right panel of Figure 5 we compare colors of red M101 cluster candidates to those of globular clusters in the Milky Way (Harris 1996), M31 (Barmby et al. 2000), and globular cluster candidates in M101 itself from Chandar et al. (2004). The median colors of M101 cluster candidates are clearly consistent with those of the globulars in the other galaxies, indicating that we have indeed detected a population of old globular clusters in M101. The larger scatter of the M101 colors presumably reflects the larger photometric or reddening-correction errors.

Figure 6 compares the joint distribution of colors and absolute magnitudes for M101, M81, and the M101 clusters found by Chandar et al. (2004). Chandar et al. (2004) were specifically attempting to select old, globular clusters in M101, while Chandar et al. (2001a) were searching only for ‘compact’ star clusters in M81 with no selection on age. The effect of our I -band magnitude cut is particularly clear in the right-hand panel of this figure: our cluster sample is missing faint, blue clusters. It is clear that the excess of red clusters in M81 compared to M101 is mostly at brighter cluster luminosities: brighter than $M_V = -7.4$ (the expected peak of the globular cluster luminosity function), the M81 clusters are mostly red, while the M101 clusters are mostly blue. We also confirm the detection by Chandar et al. (2004) of a number of faint, red clusters in M101. Some of these could be faint background galaxies, especially ellipticals or the bulges of spirals whose disks are too faint to observe. Such contamination is unlikely to account for all of the faint red clusters, whose nature is discussed further in Section 3.2.

The cluster candidate luminosity distribution is shown in Figure 7, for the full sample and the red and blue subsamples. The strong fall-off at $V > 23$ ($M_V > -6.1$) is due to our

imposed magnitude limit (see above). Brighter than this limit, we find that the blue clusters are about 0.25 mag brighter in the median than the red clusters. From population synthesis models, such a difference is consistent with the blue clusters being younger, by a few Gyr if both populations are $\gtrsim 8$ Gyr old, or less if the clusters are younger. Inferred ages are of course strongly dependent on additional factors such as metallicity, reddening, and initial mass function. As discussed below, there are many more red clusters than the expected number of globular clusters for a galaxy of M101’s luminosity: the smooth curve in the left panel of the figure shows a ‘standard’ globular cluster luminosity function (a Gaussian with mean $M_V = -7.4$ and standard deviation $\sigma = 1.3$) scaled to the number of clusters with $M_V < -7.4$ (also see Section 3.2). The bright end of the LF for the full sample is consistent with the power-law distribution of luminosity $dN(L)/dL \propto L^{-2}$ ($N(L) \propto L^{-1}$), similar to the distributions seen for young clusters in mergers (Whitmore et al. 1999; Miller et al. 1997) and *HST*-identified (not necessarily young) clusters in other spirals (Larsen 2002), as well as the bright end of the GCLF for the Milky Way and M31 (Harris & Pudritz 1994; McLaughlin 1994).

3.2. Cluster populations and spatial distribution

Do the blue and red subsamples of M101 correspond to ‘young’ and ‘globular’ cluster groups? One way to find out is to compare the number of clusters per unit galaxy luminosity in M101 to values for other galaxies. The total magnitudes of M101 as given by de Vaucouleurs et al. (1991) are $B_T = 8.31$, $V_T = 7.86$, corresponding to luminosities of $M_B = -20.82$, $M_V = -21.27$. The ‘young massive cluster’ (YMC) criterion used by Larsen & Richtler (1999) in their analysis of such clusters in nearby spirals includes both color ($B - V < 0.45$) and faint magnitude limits, $M_V < -8.5$ (the latter to avoid contamination by individual massive stars). 140 of our candidates meet these criteria, giving a value of $T_N = N_{\text{YMC}} \times 10^{0.4(M_B+15)} = 0.66$. This is a fairly typical value for spirals in the Larsen & Richtler (1999) survey: although M101 has more YMCs than all but one of the Larsen & Richtler (1999) galaxies, it is also more luminous than any of them. Only the brightest M101 blue clusters are YMCs. To compare the overall cluster population to other spirals we can use Σ_{cl}^{-8} , the number density of clusters per kpc² per 1 magnitude bin at $M_V = -8$ (defined by Larsen 2002). M101 has $\Sigma_{\text{cl}}^{-8} = 1.0$, which is quite typical of spirals.

Globular cluster populations in different galaxies are usually compared by means of the specific frequency, defined as $S_N = N_{\text{GC}} 10^{0.4(M_V+15)}$. If we assume that all 1043 red objects are globular clusters, the corresponding globular cluster specific frequency of M101 is $S_N = 3.0$. This value is quite high compared to other spiral galaxies, which typically

have values in the range 0.5–1.0 (Barmby 2003; Chandar et al. 2004), so assuming M101 to be a typical spiral would tend to support the argument that the faint red clusters are not globulars. As another estimate of S_N in M101, we can *assume* that the M101 globular clusters have the usual Gaussian luminosity function with a peak at $M_V = -7.4$ (following Chandar et al. 2004), that our cluster selection is complete to this magnitude limit, and that all red clusters brighter than this limit are true globulars. There are 160 such clusters, so if the luminosity function assumption is correct, $S_N = (320/1043) \times 3.0 = 0.9$, a much more typical value for spiral galaxies, although still higher than the 0.5 ± 0.2 found for late-type spirals by Chandar et al. (2004). These authors found $S_N = 0.4 \pm 0.1$ for M101 specifically; however, this is an extrapolation from a small number of detected globulars (29).

Are M101’s ‘excess’ faint red clusters low-mass old globulars which (unlike in earlier-type spirals) have not been destroyed by dynamical effects? Or are they instead reddened young clusters? At least some are likely to be true old clusters, since Chandar et al. (2004) found a similar population after using U -band information to eliminate younger clusters from their sample. However, since we use only BVI colors, we suspect that the majority of our faint red clusters are likely to be reddened younger clusters. The HI map upon which the column density map is based has a resolution of $\sim 15''$ (the beam was $13'' \times 16''$) while the resolution of the 12m CO map was $\sim 55''$. Since young clusters are often associated with current star-formation and localized concentrations of neutral and molecular gas, the low spatial resolution of the column density map could cause the reddening of younger clusters to be underestimated. If we have underestimated the reddening of some clusters, their absolute magnitudes would also be underestimated: correcting for this effect would then imply that the faint red clusters were intrinsically brighter than the faint blue clusters. This is a selection effect rather than a physical difference, however: more heavily-reddened clusters must be intrinsically brighter to be observable (for a discussion of this effect in M31, see Barmby et al. 2002). Given the similarity of the luminosity functions of faint red and blue clusters (see previous section), we believe it more likely that the faint red clusters are mostly reddened younger clusters.

Next we consider the spatial distribution of the M101 clusters. Using the results of the artificial cluster experiments described above, we made a ‘completeness map’, which accounts for both the spatially-varying completeness and the area on the sky actually observed as a function of distance from the center of M101. As Figure 1 shows, our observations cover most of the central $5'$ (9.75 kpc) radius of the galaxy, but only a small fraction of the region between 5 and 10 arcmin. In a set of annular bins, we counted the observed number of clusters and divided by the completeness-corrected, observed area of the annuli. The cluster candidate surface density distribution is shown in Figure 8. For comparison we also show the surface density distributions of young massive clusters in four spirals from Larsen &

Richtler (1999, their Figure 8), and of Milky Way globular clusters, using positions from Harris (1996) projected on to the plane of the Galaxy.

The overall normalization of the cluster surface density distribution in M101 is higher than in the Milky Way. This is not unexpected since the latter includes only globular clusters. However, the shape of the distribution is also different in M101: while the Milky Way globulars show a power-law distribution $n(R) \propto R^{-\alpha}$, $\alpha \sim -1.5$, the M101 and young massive cluster distributions look much more like King profiles, with a constant density core and rapid fall-off beyond. This is consistent with the M101 and other young massive clusters mostly belonging to the galaxy disks rather than the more extended halo usually identified with globular clusters.

3.3. Size distribution

We measured cluster candidate sizes using the ISHAPE program (Larsen 1999). This software fits a number of PSF-convolved model light distributions to the images of individual objects. We fit a King model with concentration index $c = 30$, for the most direct comparison with the results of Larsen (1999), although the derived effective radius is not particularly sensitive to the model chosen. We fit only circular models, as experiments showed that using elliptical light models did not significantly change the measured sizes but did increase the computing time by a factor of ~ 3 . The distribution of cluster candidate effective radii R_e (the radius which contains half of the integrated light) is shown in Figure 9. The median R_e was 2.2 ACS pixels, or 3.5 pc, which confirms that our selection procedure did indeed select mostly slightly extended objects. Fewer than 10% of our candidates were flagged as ‘possibly stellar’ by ISHAPE.

There is a difference in the size distributions of red and blue clusters. The red clusters, with a median $R_e = 4.1$ pc, are slightly larger than the blue clusters, whose median size is 3.2 pc. Dynamical studies of star cluster evolution (e.g. Gnedin & Ostriker 1997) show that large clusters are more easily destroyed, so we expected that the red (older) clusters would be slightly smaller on average than the blue (younger). However, since the clusters are only marginally resolved, the difference between the two groups is not of major significance and could reflect contamination of the red cluster sample by younger clusters or galaxies. The range of blue cluster candidate sizes is similar to the range found by Larsen (1999) for ‘young massive clusters’ and is also comparable to the median half-light radius for Milky Way globular clusters $R_e = 3.2$ pc (Harris 1996).

4. Summary

We have presented the results from an initial search for star clusters in Hubble Space Telescope/Advanced Camera for Surveys images of the nearby giant spiral M101. Defining a reliable sample of cluster candidates in these complex, crowded images proved to be a challenge. Our final cluster candidate list contains nearly 3000 objects of which a majority are blue and associated with the galaxy's spiral arms. These cluster candidates have color distributions similar to candidates and confirmed clusters in other spirals including the Milky Way, M31, M81, M33, and M51. M101 has fewer bright, red clusters than the earlier-type spiral M81, but many more faint red clusters (as originally noted by Chandar et al. 2004). If all of these faint red clusters were globulars, M101 would have a much higher globular cluster specific frequency and a much different globular cluster luminosity function from other galaxies. We suggest that many of the red M101 clusters are likely to be reddened young clusters, which is supported by the consistency of the overall cluster luminosity distribution and fiducial cluster density with those found in other spirals by Larsen (2002). The spatial distribution of the M101 clusters shows a relatively flat core and a steep drop-off at larger galactocentric distances, suggesting that the clusters are associated with the galaxy disk rather than its halo. The size distributions of the M101 cluster candidates show them to be slightly resolved, as expected, and are consistent with cluster sizes measured in other galaxies.

Support for program GO-9490 was provided by NASA through a grant from the Space Telescope Science Institute, which is operated by the Association of Universities for Research in Astronomy, Inc., under NASA contract NAS 5-26555.

REFERENCES

- Barmby, P. 2003, in *Extragalactic Globular Cluster Systems*, ed. M. Kissler-Patig (Berlin: Springer-Verlag), 143
- Barmby, P., Huchra, J. P., Brodie, J. P., Forbes, D. A., Schroder, L. L., & Grillmair, C. J. 2000, *AJ*, 119, 727
- Barmby, P., Perrett, K. M., & Bridges, T. J. 2002, *MNRAS*, 329, 461
- Bertin, E. & Arnouts, S. 1996, *A&AS*, 117, 393
- Bica, E., Dutra, C. M., Soares, J., & Barbuy, B. 2003, *A&A*, 404, 223

- Bik, A., Lamers, H. J. G. L. M., Bastian, N., Panagia, N., & Romaniello, M. 2003, *A&A*, 397, 473
- Bohlin, R., Savage, B., & Drake, J. 1978, *ApJ*, 224, 132
- Bresolin, F., Kennicutt, R. C., & Stetson, P. B. 1996, *AJ*, 112, 1009
- Chandar, R., Ford, H. C., & Tsvetanov, Z. 2001a, *AJ*, 122, 1330
- Chandar, R., Tsvetanov, Z., & Ford, H. C. 2001b, *AJ*, 122, 1342
- Chandar, R., Whitmore, B., & Lee, M. G. 2004, *ApJ*, 611, 220
- de Vaucouleurs, G., de Vaucouleurs, A., Corwin, H. G., Buta, R. J., Paturel, G., & Fouque, P. 1991, *Third Reference Catalogue of Bright Galaxies (RC3)* (New York: Springer-Verlag)
- Ford, H. et al. 2002, *SPIE*, 4854, 81
- Freedman, W. L. et al. 2001, *ApJ*, 553, 47
- Gnedin, O. Y. & Ostriker, J. P. 1997, *ApJ*, 474, 223
- Goudfrooij, P., Strader, J., Brenneman, L., Kissler-Patig, M., Minniti, D., & Huizinga, J. 2003, *MNRAS*, 343, 665
- Harris, W. E. 1996, *AJ*, 112, 1487
- Harris, W. E. & Pudritz, R. E. 1994, *ApJ*, 429, 177
- Kelson, D. D. et al. 1996, *ApJ*, 463, 26
- Krist, J. 1995, in *Astronomical Data Analysis Software and Systems IV*, ed. R. Shaw, H. Payne, & J. Hayes, *ASP Conf. Ser.*, 349
- Kundu, A. & Whitmore, B. C. 1998, *AJ*, 116, 2841
- Kuntz, K. D., Gruendl, R. A., Chu, Y.-H., Chen, C.-H. R., Still, M., Mukai, K., & Mushotzky, R. F. 2005, *ApJ*, 620, L31
- Kuntz, K. D., Snowden, S. L., Pence, W. D., & Mukai, K. 2003, *ApJ*, 588, 264
- Larsen, S. S. 1999, *A&AS*, 139, 393
- Larsen, S. S. 2002, *AJ*, 124, 1393

- Larsen, S. S. & Richtler, T. 1999, *A&A*, 345, 59
- Lee, M. G., Chandar, R., & Whitmore, B. C. 2005, *AJ*, 130, 2128
- McLaughlin, D. E. 1994, *PASP*, 106, 47
- Miller, B. W., Whitmore, B. C., Schweizer, F., & Fall, S. M. 1997, *AJ*, 114, 2381
- Mochejska, B. J., Kaluzny, J., Krockenberger, M., Sasselov, D. D., & Stanek, K. Z. 1998, *Acta Astronomica*, 48, 455
- Mukai, K., Pence, W. D., Snowden, S. L., & Kuntz, K. D. 2003, *ApJ*, 582, 184
- Shafter, A. W., Ciardullo, R., & Pritchett, C. J. 2000, *ApJ*, 530, 193
- Sirianni, M. et al. 2005, *PASP*, 117, 1049
- Stetson, P. B. et al. 1998, *ApJ*, 508, 491
- Strader, J., Brodie, J. P., Cenarro, A. J., Beasley, M. A., & Forbes, D. A. 2005, *AJ*, 130, 1315
- Whitmore, B. C., Zhang, Q., Leitherer, C., Fall, S. M., Schweizer, F., & Miller, B. W. 1999, *AJ*, 118, 1551

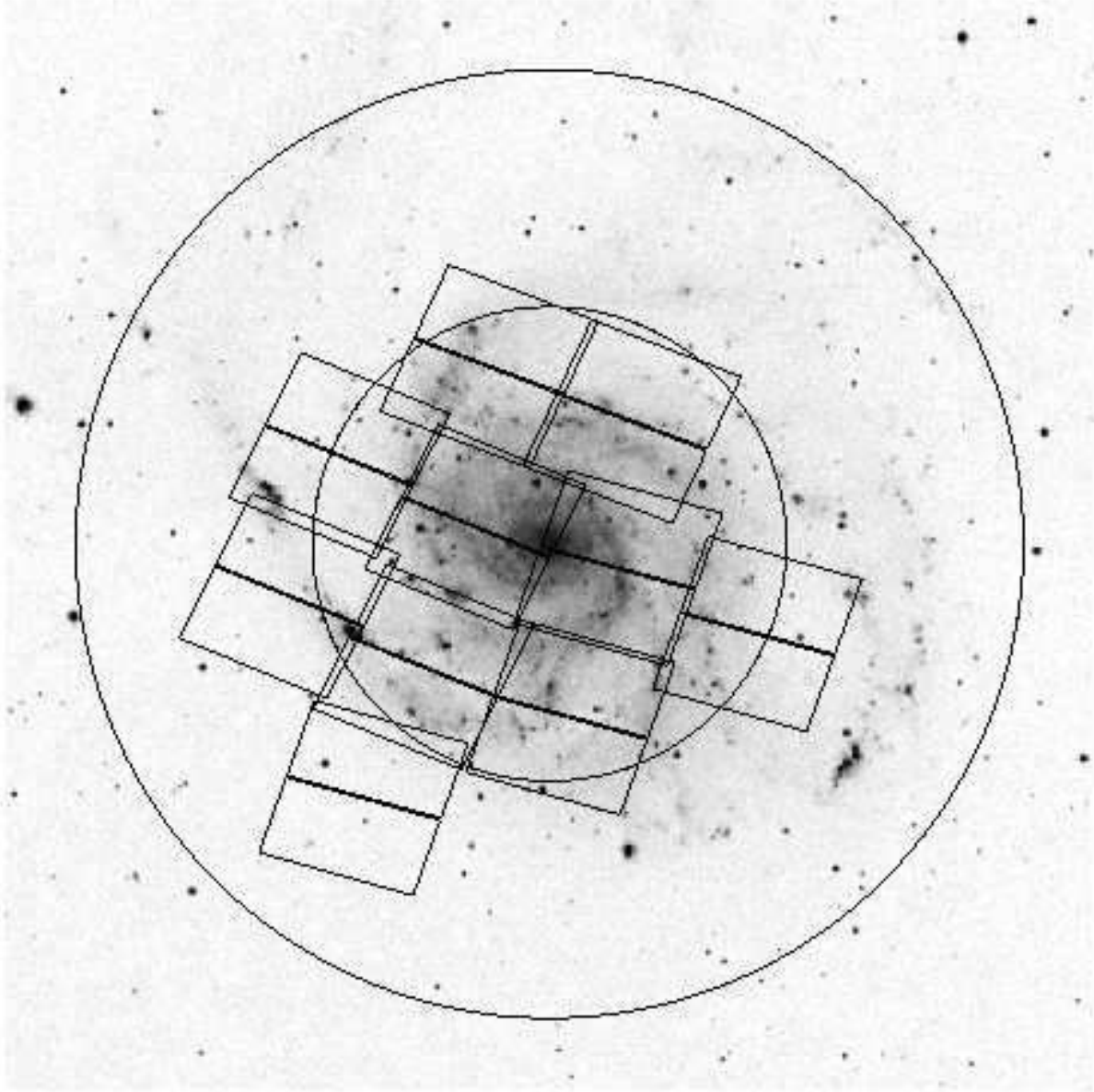


Fig. 1.— Location of ACS fields in M101, overplotted on a Digitized Sky Survey image. North is up and East to the left. The two circles are centered on the galaxy and have radii of 5 and 10 arcminutes, or 9.75 and 19.5 kpc at the distance of M101 (6.7 Mpc; Freedman et al. 2001).

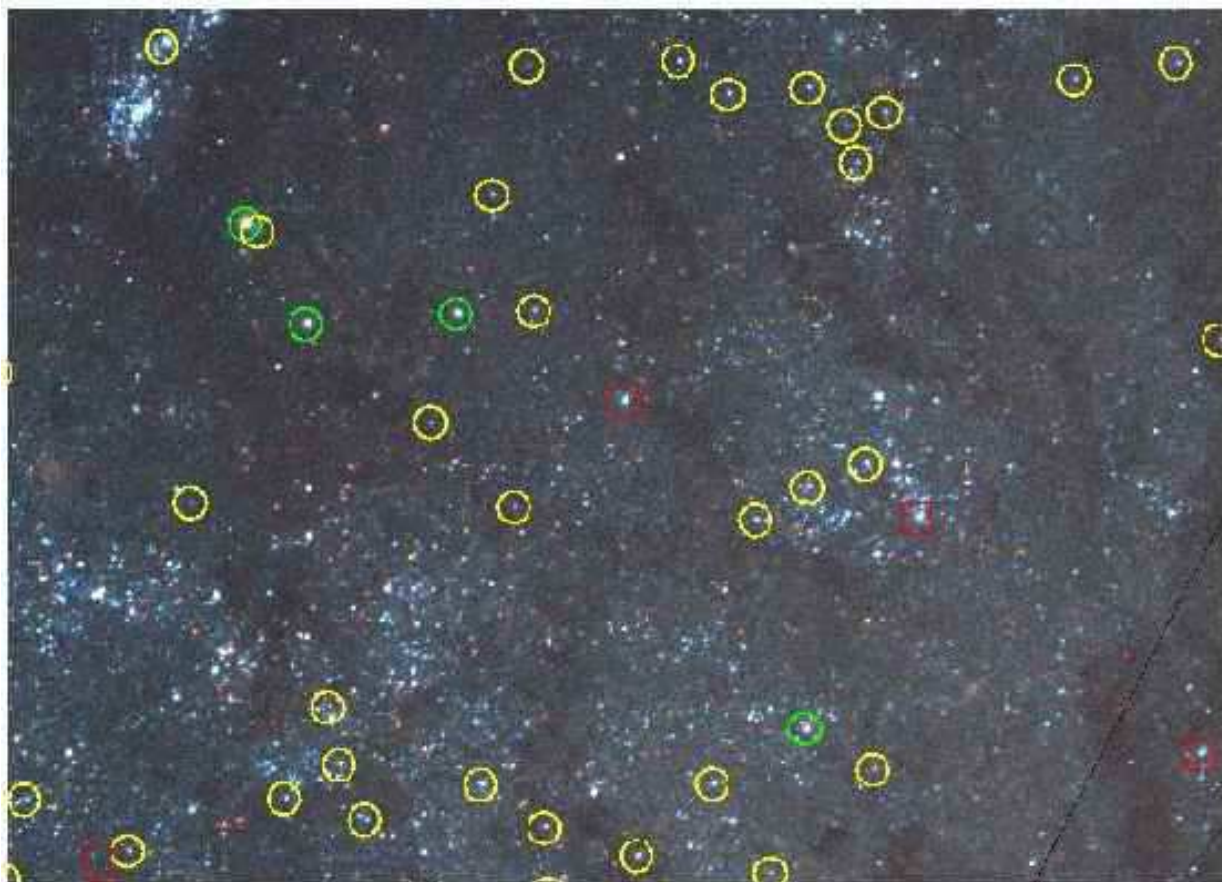


Fig. 2.— Three-color view of a portion ($1'.0 \times 0'.7$) of one ACS field, centered at position $14^{\text{h}}03^{\text{m}}27$, $54^{\circ}22'13''$ (J2000). North is up and east to the left. The F435W filter is blue, F555W is green, F814W is red. Yellow circles are cluster candidates selected from the ACS data, green circles are cluster candidates selected from the ACS data and by Bresolin et al. (1996), and red squares mark candidates selected by Bresolin et al. (1996) but not in the present work.

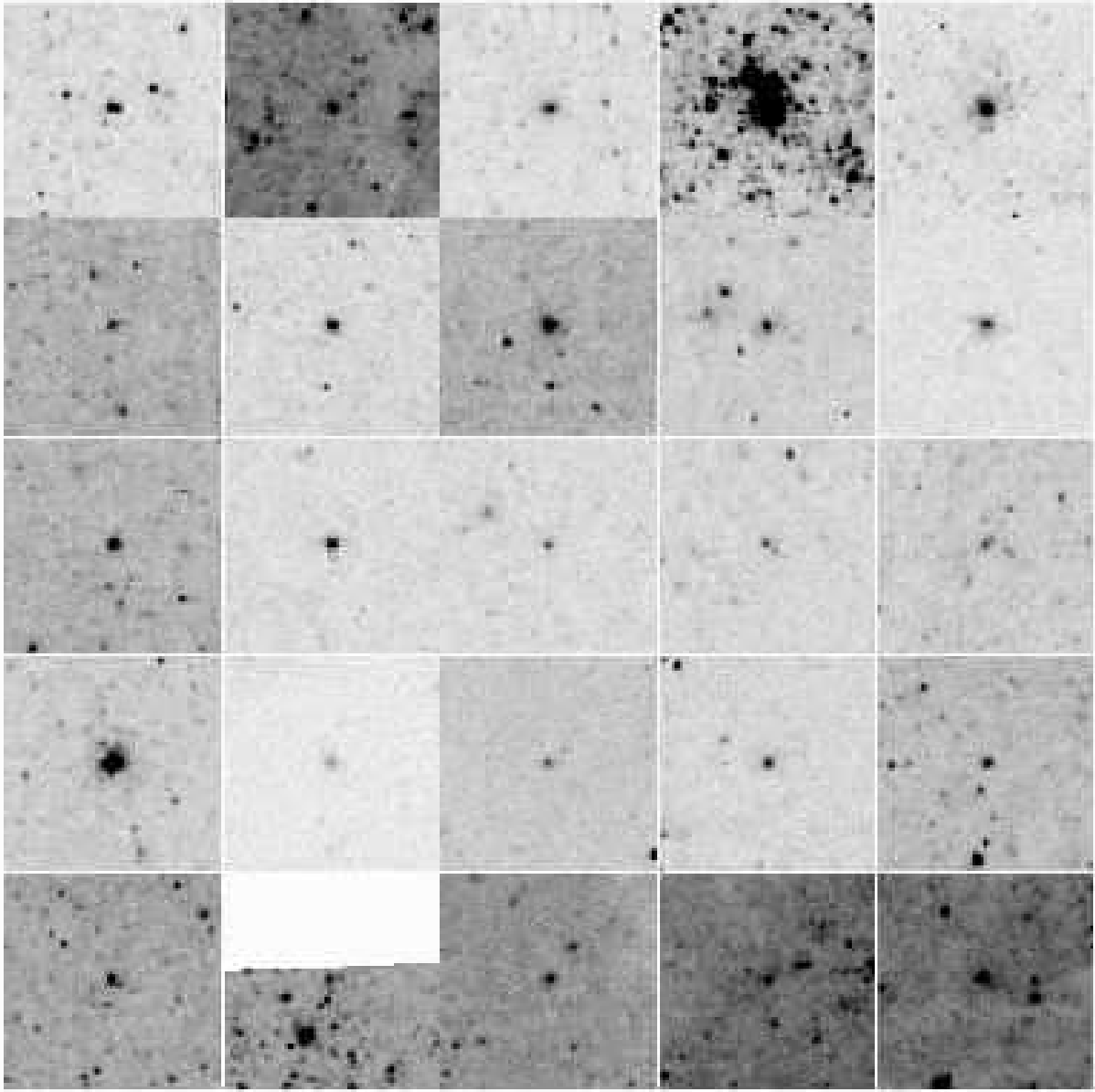


Fig. 3.— Images of 25 randomly-chosen M101 cluster candidates. Each image is $5''.05 \times 5''.05$ (101 ACS WFC pixels).

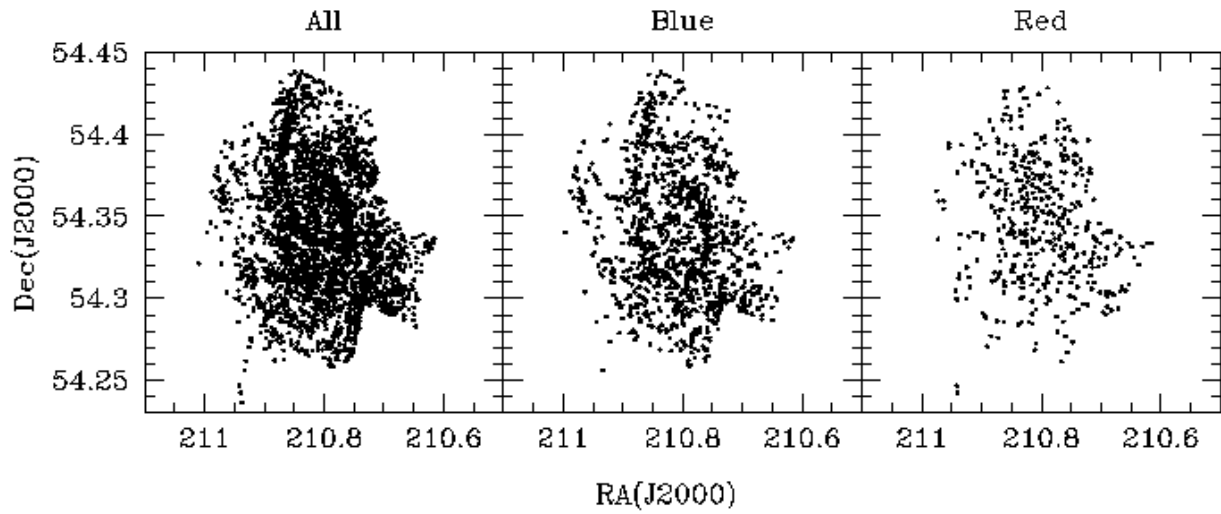


Fig. 4.— Spatial distribution of M101 cluster candidates. The left panel contains all 2920 candidates, while the right two panels show the red and blue clusters separately. They contain only clusters with $V < 23$, for which the sample is not biased by color.

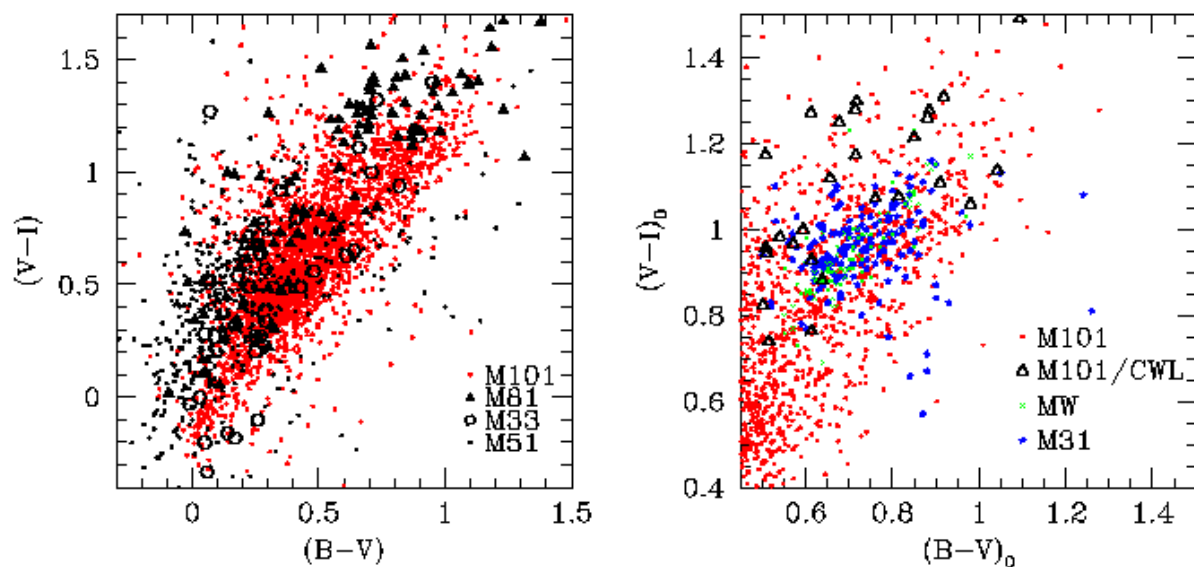


Fig. 5.— Two-color plot for (candidate) clusters in spiral galaxies. Left: observed colors (not de-reddened) for M101 cluster candidates from this work (small red dots), M51 cluster candidates (small black dots; Bik et al. 2003), M81 cluster candidates (filled triangles; Chandar et al. 2001a), and M33 cluster candidates (open circles; Mochejska et al. 1998). Right: color distribution for red clusters, de-reddened. M101 cluster candidates from this work (small red dots), M101 globular cluster candidates (open triangles; Chandar et al. 2004), Milky Way globular clusters (green crosses; Harris 1996), and M31 globular clusters (small blue stars; Barmby et al. 2000).

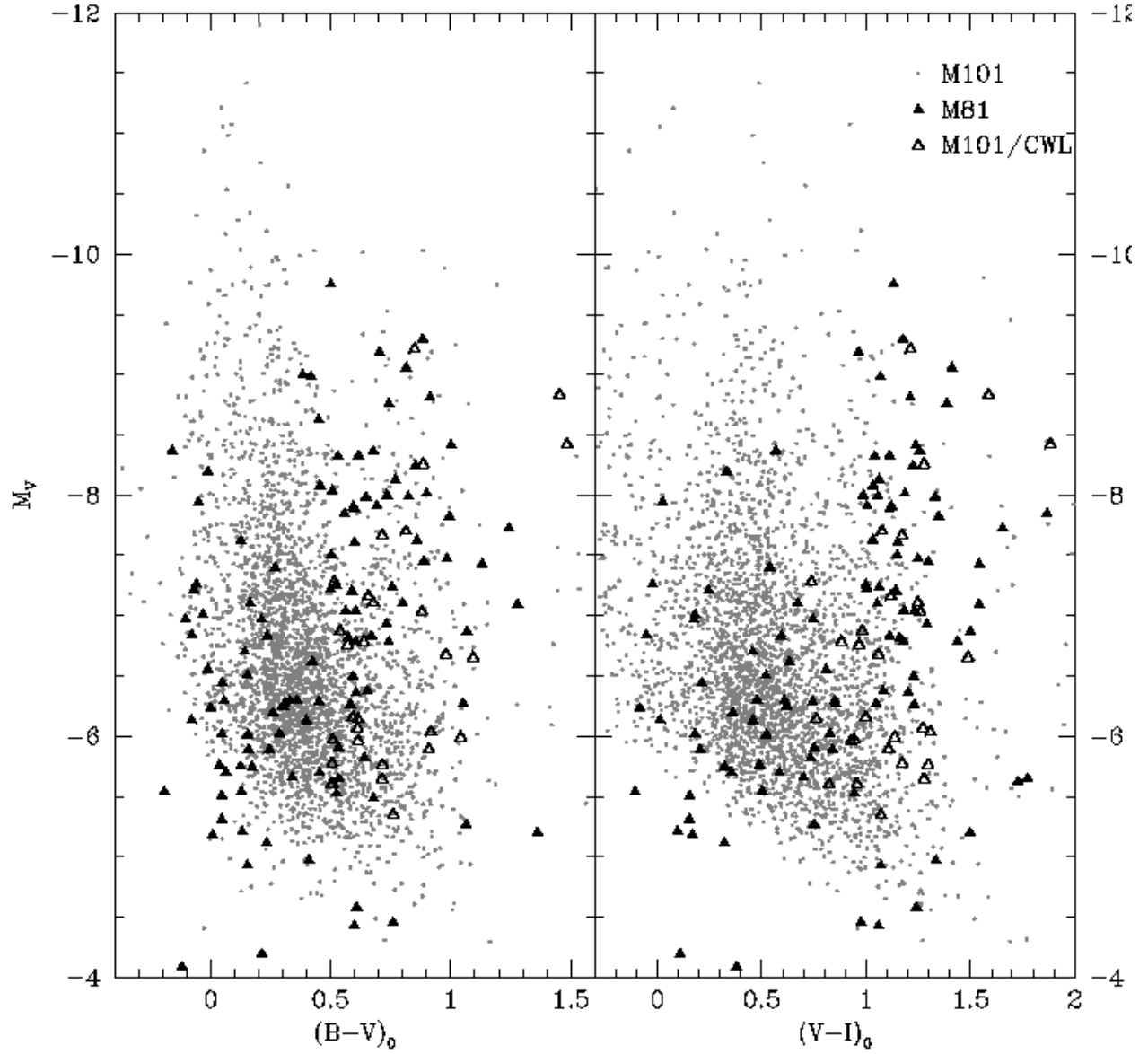


Fig. 6.— Color-magnitude diagrams for star clusters in M101 and M81. Symbols: M101 cluster candidates from this work (small grey dots), M81 cluster candidates (filled triangles; Chandar et al. 2001a), M101 globular cluster candidates (open triangles; Chandar et al. 2004).

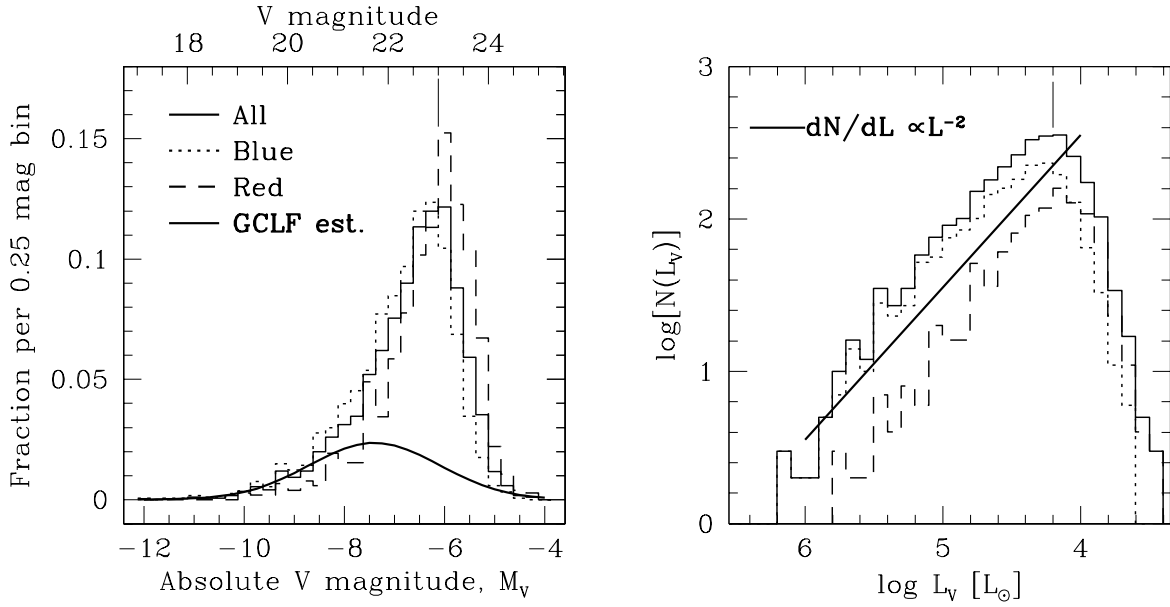


Fig. 7.— (Left) M101 star cluster candidate magnitude distributions: all clusters (solid histogram), blue clusters (dotted histogram), red clusters (short-dashed histogram). The heavy smooth curve shows the expected globular cluster luminosity function, scaled to the number of red clusters with $M_V < -7.4$. (Right) M101 star cluster candidate luminosity distributions. Line types as in left panel, except that the heavy solid line illustrates a power-law distribution $dN(L)/dL \propto L^{-2}$ (not a fit to the data). In both panels, the vertical line indicates the $V = 23$ limit below which the blue cluster sample is incomplete.

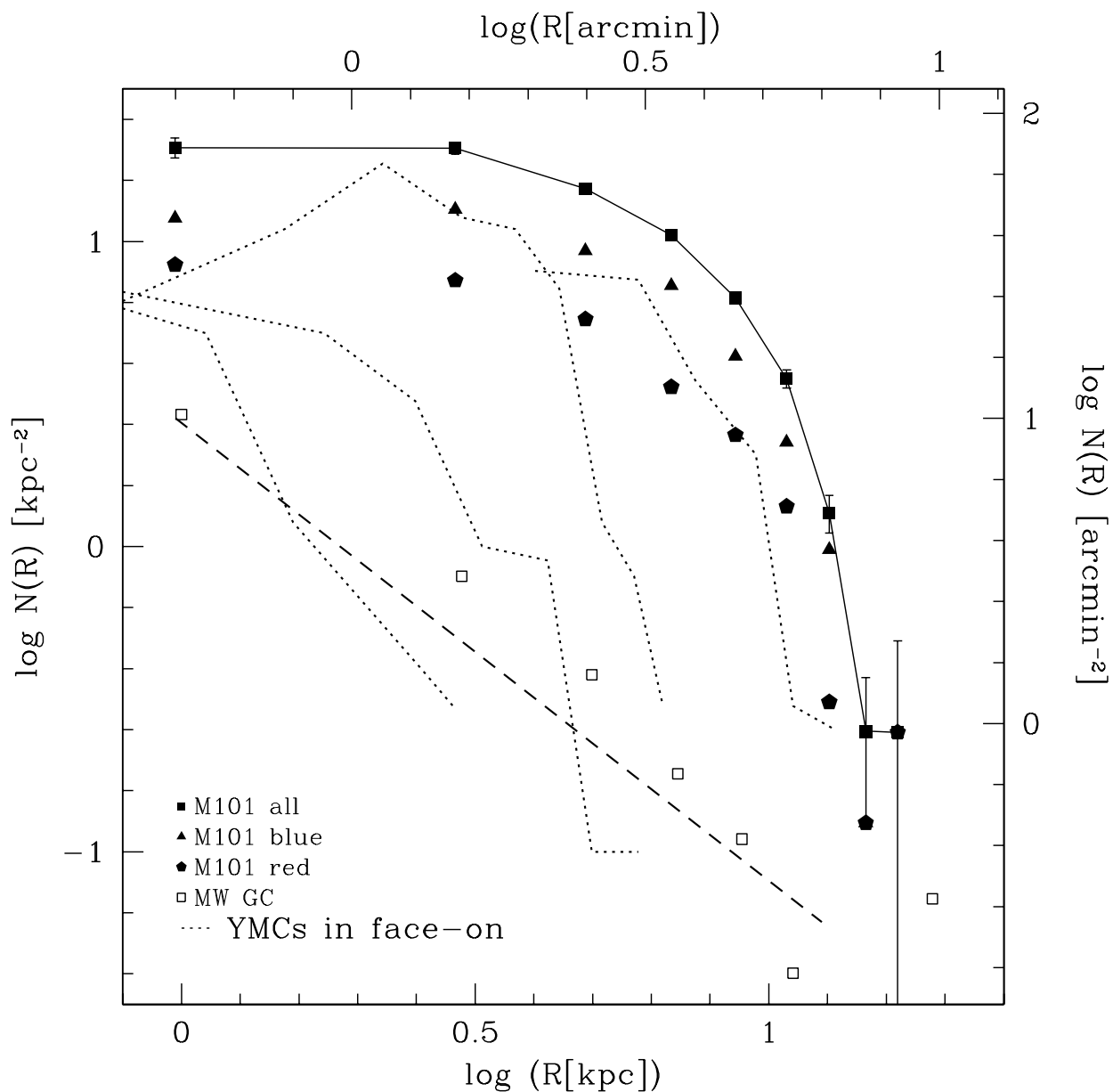


Fig. 8.— Cluster candidate surface density distribution for all M101 clusters (filled squares), M101 blue clusters (triangles), M101 red clusters (pentagons), and Milky Way globulars (open squares) Dotted lines: cluster surface density distributions in NGC 1156, NGC 1313, NGC 2997 and NGC 5236 from Larsen & Richtler (1999), with arbitrary vertical normalization. The axes labeled in kpc apply to all galaxies, while the labels in arcminutes apply only to M101. The dashed line illustrates a power-law distribution $N(R) \propto R^{-1.5}$; it is not a fit to the data for any galaxy.

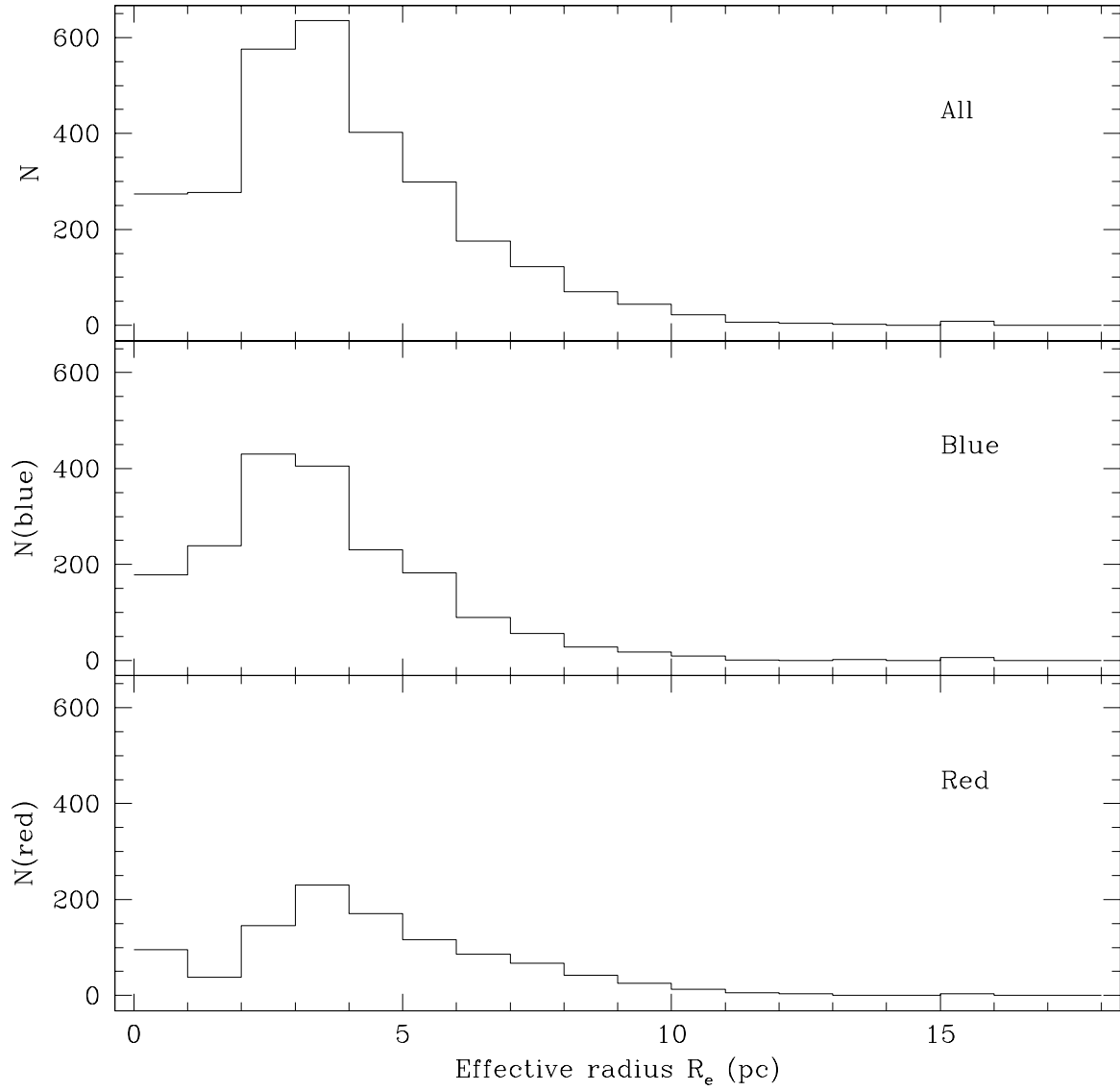


Fig. 9.— Cluster candidate effective radius distribution for all M101 cluster candidates (top), blue candidates (center), and red candidates (bottom).